JOC The Journal of Organic Chemistry

Article

pubs.acs.org/joc

Benzimidazole Conjugate of 1,1′-Thiobis(2-naphthol) as *Switch-On* Fluorescence Receptor for Ag^+ and the Complex as Secondary Recognition Ensemble toward Cys, Asp, and Glu in Aqueous Methanolic Solution: Synthesis, Characterization, Ion and Amino Acid Recognition, Computational Studies, and Microscopy Features

Jayaraman Dessingou, Atanu Mitra, Khatija Tabbasum, Garima Singh Baghel, and Chebrolu P. Rao*

Bioinorganic Laboratory, Department of Chemistry, Indian Institute of Technology Bombay, Powai, Mumbai 400076, India

Supporting Information

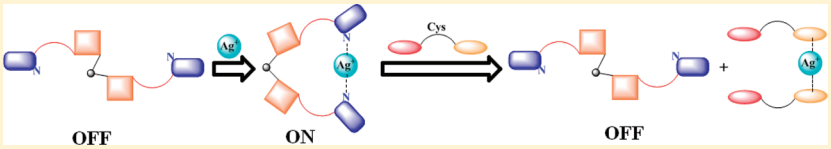

ABSTRACT: A new 1,1′-thiobis(2-naphthoxy)-based receptor molecule (**L**) containing a benzimidazole moiety has been synthesized and characterized by ^{1}H NMR, ESI-MS, and elemental analysis. The selectivity of **L** has been explored in aqueous methanol, resulting in selective (7.5 ± 0.5)-fold *switch-on* fluorescence response toward Ag^+ among 14 different transition, alkali, and alkaline earth metal ions studied. The complexation of Ag^+ by **L** has been addressed by ESI-MS, ^{1}H NMR, and UV−vis spectra. Microstructural features of **L** and its Ag^+ complex have been measured by AFM and TEM. The morphological features of **L** alone and **L** in the presence of Ag^+ differ dramatically both in shape and size, and the ion induces the formation of chains owing to its coordinating ability toward benzimidazole. Further, the in situ [Ag^+−**L**] complex was titrated against 20 naturally occurring amino acids and found that this complex acts as a secondary recognition ensemble toward Cys, Asp, and Glu by *switch-off* fluorescence.

INTRODUCTION

Selective recognition of Ag^+ ions and amino acids is an important area of research due to their involvement in chemical, biological, and environmental applications.[1] Silver compounds are used as antimicrobial agents, and the activity is closely related with the interaction of Ag^+ with sulfhydryl (−SH) groups.[2] There are several chemosensors reported in the literature for the recognition of Ag^+ ion in nonaqueous[3] and aqueous[4] systems. However, the molecular receptors which can recognize Ag^+ followed by amino acids are indeed limited in the literature. A calix[4]arene derivative possessing a picolyl moiety has been shown to selectively recognize Ag^+ ion and also act as a secondary sensor toward cysteine.[5] Receptors with benzimidazole moieties can be used as sensors for ion recognition in aqueous environment. A bis-benzimidazole-based N,S macrocycle[6] has been shown to be a sensor for metal ions such as Cr^{2+}, Fe^{2+}, Co^{2+}, Ni^{2+}, Cu^{2+}, Zn^{2+}, Hg^{2+}, and Pb^{2+} in aqueous phase, and it is not selective for specific metal ions. Another Ag^+ complex of pyridyl benzimidazole[7] is shown to be a fluorescent complex, where the Ag^+ is coordinated in a polymeric fashion by exhibiting a distorted "T" shape geometry. The metal ion sensors with di-O-derivatives of the thiobisnaphthol receptor are scarce in the literature and hence are least explored. Thiobisnaphthol derivatives have been shown to be sensitive for metal ions, such as Ag^+, Hg^{2+}, Cr^{3+}, Pb^{2+}, and Ni^{2+} by absorption spectroscopy, but these are not specific for a single metal ion.[8] It is always of interest to explore the recognition properties of difunctionalized 1,1′-thiobis(2-naphthol) and much more so if it can act as a dual sensor by exhibiting primary followed by the secondary sensing properties. Therefore, the present study reports the synthesis, characterization, and Ag^+-recognition properties of an amido conjugate of benzimidazole of 1,1′-thiobis(2-naphthol) (**L**), followed by the recognition of Cys, Asp, and Glu by the corresponding silver complex.

RESULTS AND DISCUSSION

The receptor molecule, **L**, was synthesized in four steps (Scheme 1). The reaction of $\mathbf{L_1}$ with ethyl bromoacetate results in the formation of diester derivative, $\mathbf{L_2}$, and its hydrolysis under basic conditions yielded the corresponding diacid derivative, $\mathbf{L_3}$. The diacid $\mathbf{L_3}$, upon coupling with 2-amino-methylbenzimidazole using 1-ethyl-(3-dimethylaminopropyl)-3-carbodiimide hydrochloride, resulted in **L**. The control molecule $\mathbf{L_4}$ (Scheme 1) has also been synthesized by coupling of 2-aminomethylbenzimidazole with phenoxyacetic acid using the same reagent. All of the compounds exhibited satisfactory analytical and spectral data as given in the Experimental Section (Supporting Information SI 01−04). The metal ion receptor

Received: September 26, 2011
Published: November 21, 2011

   dx.doi.org/10.1021/jo201926q | *J. Org. Chem.* 2012, 77, 371−378

Scheme 1. Synthesis of Control and Receptor Molecules[a]

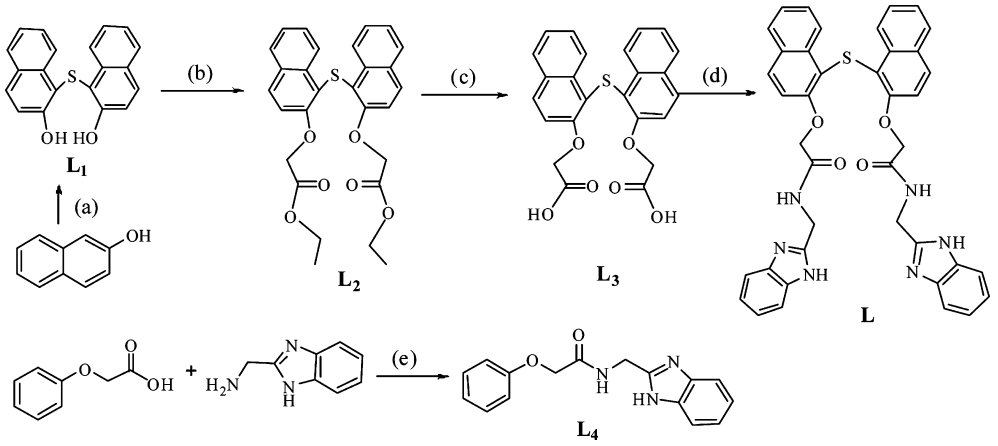

[a]Conditions: (a) SCl_2, $(CH_3CH_2)_2O$, rt/24 h; (b) $BrCH_2COOC_2H_5/K_2CO_3$/acetone/reflux/12 h; (c) 15% NaOH/EtOH/reflux/24 h; (d) 1-ethyl-(3-dimethylaminopropyl)-3-carbodiimide hydrochloride/aminomethyl benzimidazole hydrochloride/DMF/rt/12 h; (e) 1-ethyl-(3-dimethylamino-propyl)-3-carbodiimide hydrochloride/CH_2Cl_2/rt/12 h.

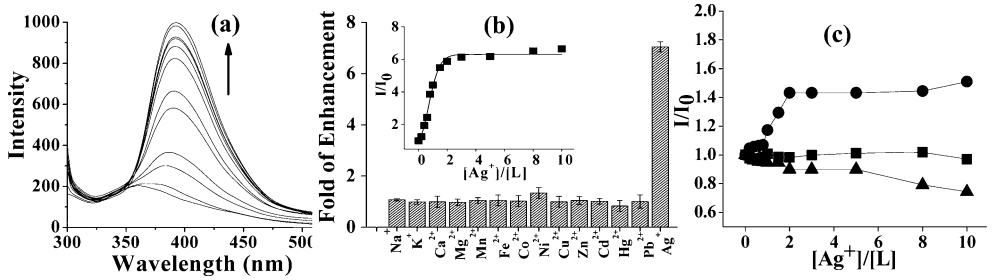

Figure 1. (a) Fluorescence spectral traces of **L** in MeOH/H_2O (2:3 v/v ratio) as a function of added Ag^+ to result in $[Ag^+]/[L]$ mole ratio from 0 to 10.0. (b) Histogram of fluorescence enhancement folds in the presence of different metal ions when titrated against **L**. Inset: Relative fluorescence intensity (I/I_0) vs $[Ag^+]/[L]$ mole ratio at 390 nm. (c) Plot of I/I_0 vs mole ratio of Ag^+/[ligand] at 372 nm for L_1 (squares), 365 nm for L_2 (circles), and 300 nm for L_4 (triangles).

property of **L** was explored by carrying out fluorescence titrations of 14 different ions (Figure 1a,b), including alkali, alkaline earth, and transition ones, viz., Na^+, K^+, Ca^{2+}, Mg^{2+}, Mn^{2+}, Fe^{2+}, Co^{2+}, Ni^{2+}, Cu^{2+}, Zn^{2+}, Cd^{2+}, Hg^{2+}, Pb^{2+}, and Ag^+ with perchlorate as counteranion. Among all of these ions (SI 05), only Ag^+ showed fluorescence enhancement as a function of the addition of increasing concentrations of this ion, and the enhancement approaches (7.5 ± 0.5)-fold at saturation when the titration was carried out in methanol/water in 2:3 v/v ratio (Figure 1b). During the titration, the emission band observed at 360 nm is shifted to red by 30 nm upon the interaction with Ag^+ (Figure 1a). Plot of relative fluorescence intensity (I/I_0) versuss $[Ag^+]/[L]$ mole ratio suggests the formation of a 1:1 complex and hence is stoichiometric. The association constant obtained for the $[Ag^+–L]$ complex has been found to be 40 660 ± 200 M^{-1} using the Benesi–Hildebrand equation. The quantum yield found with respect to the naphthalene as a standard is 0.016 and 0.071 for **L** and $[Ag^+–L]$, respectively. Minimum detection limit of Ag^+ by **L** using fluorescence titration has been found to be 430 ± 50 ppb (SI 06). In order to substantiate the unique nature of the interaction of Ag^+ with **L** (i.e., through benzimidazole moiety), three related control molecular systems, viz., L_1, L_2, and L_4 were subjected to similar fluorescence titration studies (SI 07). The control molecules L_1 and L_2 do not show any considerable extent of fluorescence enhancement, suggesting the positive role of the benzimidazole moiety in the recognition process (Figure 1c). On the other hand, the L_4 possessing the benzimidazole moiety exhibits fluorescence emission at 300 nm as the same is devoid of the thiobisnaphthyl moiety and exhibits a considerable quenching of fluorescence upon titration with Ag^+ (SI 07, Figure 1c). On the basis of the fluorescence titration data, the association constant of Ag^+ with L_4 has been found to be 8550 ± 150 M^{-1}, which is ~5 times less than that obtained between **L** and Ag^+.

In order to explore the effect of polarity of the solvent on the emission intensity, fluorescence titrations were carried out in different ratios of water–methanol mixtures and it was found that the changes were maximum in a 2:3 mixture (Figure 2).

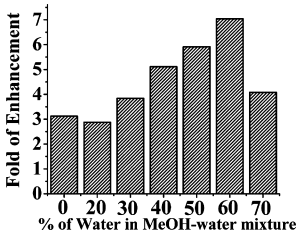

Figure 2. Histogram of fluorescence enhancement fold in various methanol–water mixtures when Ag^+ was titrated against **L**.

Such studies could not be extended to the solvent mixtures containing more than 70% of water due to the precipitation.

Competitive Ion Titrations by Fluorescence. In order to check the practical utility of Ag^+ recognition by **L**,

dx.doi.org/10.1021/jo201926q | J. Org. Chem. 2012, 77, 371–378

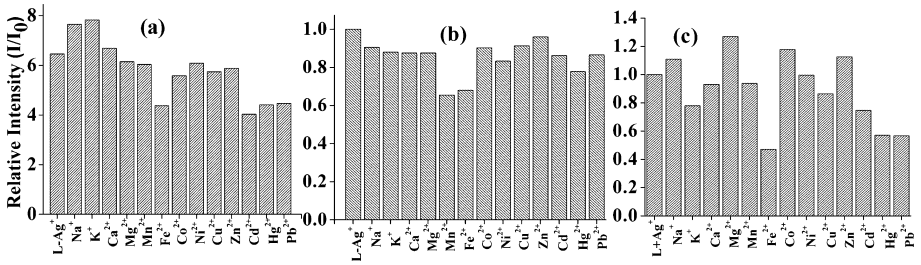

Figure 3. Histograms showing the relative fluorescence intensity (I/I_0) for the titration of **L** with Ag^+ in the presence of competitive ions: (a) titration of [**L** + *x* equiv of M^{n+}] against Ag^+; and (b) [**L** + 2 equiv of Ag^+] against M^{n+} (up to *x* equiv), where *x* = 30 for Na^+, K^+, Ca^{2+}, and Mg^{2+} and *x* = 5 for other metal ions. (b) [**L** + 1 equiv of Ag^+] against M^{n+} (up to *x* equiv), where *x* = 30 for Na^+, K^+, Ca^{2+}, and Mg^{2+} and *x* = 5 for other metal ions. (c) Similar experimental conditions as shown in (b) except that 1 equiv of Ag^+ is added in this case.

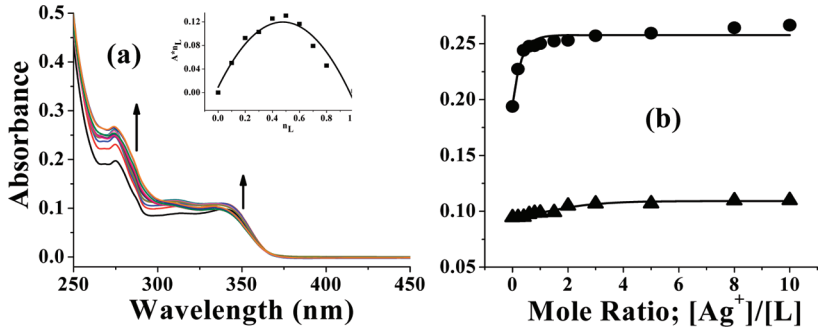

Figure 4. (a) UV−visible absorption spectral traces of **L** on titration against Ag^+. Inset: Job's plot of n_L versus $A \times n_L$, where n_L is mole fraction of the metal ion added and *A* is the absorbance. (b) Absorbance vs mole ratio plots at 340 nm (triangles) and 273 nm (circles).

competitive titrations were carried out in the presence of other biologically and ecologically relevant metal ions. Fluorescence spectra (SI 08) were recorded for the titration of **L** against Ag^+ in the presence of 30 equiv of Na^+, K^+, Ca^{2+}, and Mg^{2+} and 5 equiv of Mn^{2+}, Fe^{2+}, Co^{2+}, Ni^{2+}, Cu^{2+}, Zn^{2+}, Cd^{2+}, Hg^{2+}, and Pb^{2+}. None of these metal ions significantly affect the emission intensity of **L** upon the addition of Ag^+, and the titration profile is similar to that obtained for simple Ag^+ titration (Figure 3a). Therefore, it can be concluded that **L** recognizes Ag^+ even in the presence of other metal ions. In another titration, the in situ generated [**L** + 2 equiv of Ag^+] has been titrated with metal ions, Na^+, K^+, Ca^{2+}, Mg^{2+}, Mn^{2+}, Fe^{2+}, Co^{2+}, Ni^{2+}, Cu^{2+}, Zn^{2+}, Cd^{2+}, Hg^{2+}, and Pb^{2+}, and found to have only marginal changes in the emission intensity, suggesting that none of these ions interfere in the fluorescence emission of the Ag^+ complex (Figure 3b). The competitive titrations were also carried out with an in situ complex prepared using 1:1 of **L** and Ag^+ against other metal ions (Figure 3c). The results obtained from this experiment are almost same except in the case of Fe^{2+}, Pb^{2+}, and Hg^{2+}, where a 10−20% higher quenching was observed when compared to the earlier titration that was carried out with 1:2 ratio of **L** and Ag^+. Thus the results shown in Figure 3 indicate that Ag^+ is not being replaced by other metal ions from the binding core of **L**.

Absorption Titration of L with Ag^+. In order to ascertain the complexation of Ag^+ by **L**, absorption titrations were carried out by adding varying concentrations of Ag^+ to a fixed concentration (35 μM) of **L**. The absorbance of 273, 278, and 340 nm bands is found to increase upon addition of Ag^+ (Figure 4), indicating the interaction of Ag^+ with the benzimidazole/aromatic moiety. Further, the stoichiometry of the complex formed between **L** and Ag^+ has been found to be 1:1 based on the Job's plot.

Authenticity for the Formation of the Complex of L with Ag^+ by ESI-MS Titration. The complex formed between **L** and Ag^+ has been confirmed from the molecular ion peak observed at m/z = 801.25 in the ESI-MS spectrum (SI 09). The presence of Ag^+ has been further proven by comparing the observed isotopic peak pattern with that of the calculated one (Figure 5).

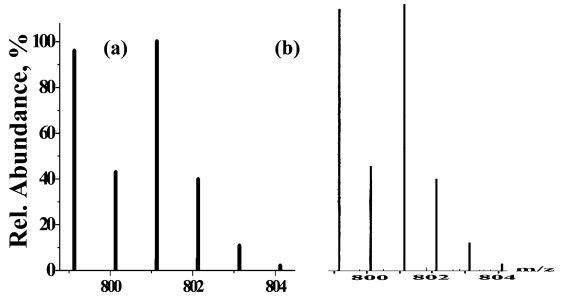

Figure 5. Molecular ion peak obtained in the titration of **L** against Ag^+ along with its isotopic peak pattern: (a) calculated, (b) experimental.

Titration of L with Ag^+ by ^1H NMR Spectroscopy. The nature of binding of Ag^+ to **L** has been further studied by ^1H NMR titration by keeping a fixed concentration of **L** and varying the amount of Ag^+ added to reach up to 2 equiv. During the titration, significant changes were observed in the ^1H NMR spectrum of **L** upon addition of Ag^+ (Figure 6). The benzimidazole −NH proton signals of **L** observed at 12.20 ppm are found to shift downfield by about 1.0 ppm, indicating the involvement of the benzimidazole moiety in Ag^+ binding. Aromatic signals of the benzimidazole moiety (8.2−8.6 ppm) further split into two peaks in the presence of Ag^+ that may arise from the loss of symmetry upon interaction of **L** with Ag^+.

dx.doi.org/10.1021/jo201926q | J. Org. Chem. 2012, 77, 371−378

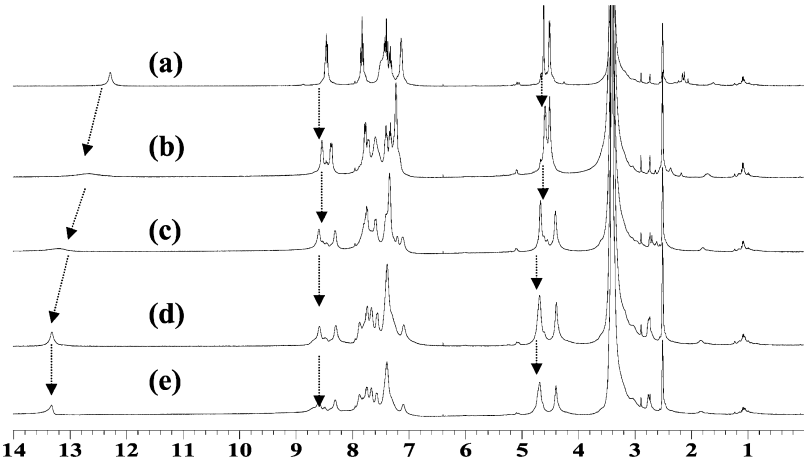

Figure 6. ^{1}H NMR spectra measured during the titration of **L** with different equivalents of Ag^+ (in DMSO-d_6): (a) 0; (b) 0.5; (c) 1.0; (d) 1.5; (e) 2.0.

Aromatic signals of the naphthyl moiety (7−8 ppm) are also found to change upon addition of Ag^+. Both the $-OCH_2$ and $-NH-CH_2$ protons show shifts in their signals, viz., from 4.6 to 4.7 and 4.5 to 4.4 ppm, respectively, which further suggests the interaction of Ag^+ with the groups present on both arms. The changes observed in the proton signals upon Ag^+ addition ($\Delta\delta$) are given in Figure 7.

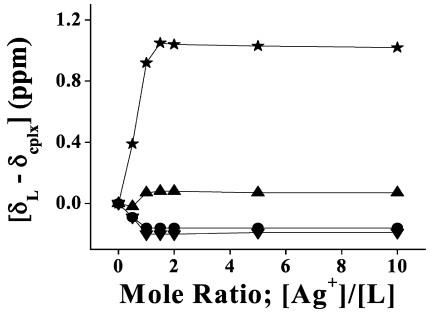

Figure 7. Metal ion induced shifts ($\Delta\delta = \delta_L - \delta_{cplx}$) observed with different protons of **L** at various mole ratios of $[Ag^+]/[L]$. The labeling for various protons can be seen from the structure: (★) benzimidazole-NH; (●) benzimidazole-aromatic-CH; (▲) OCH_2; (▼) $NH-CH_2$.

Structural Features of the [Ag$^+$−L] Complex by DFT Computational Studies. As the formation of a 1:1 species was already established by absorption, fluorescence, and ESI-MS, the structural features of the complex formed between **L** and the Ag^+ were addressed by computational studies. The results of the complex obtained at B3LYP/3-21G were reported in this paper. At the B3LYP/3-21G level of computation, the complex $[Ag^+-L]$ was mainly formed through the interaction of two benzimidazole N atoms of **L** giving rise to a near linear geometry for Ag^+ (N1−Ag−N2 = 169°) with N1−Ag = 2.17 Å and N2−Ag = 2.20 Å (Figure 8, SI 10). One of the amide−C═O exhibits a weak interaction as the amide-O···Ag distance, 2.66 Å, is lower than the sum of the van der Waal's radii of O and Ag. At this level of computation, the stabilization energies computed using the formula $\Delta E_s = E_c - [E_L + E_{Ag}]$ (where E_c is the total energy of the complex, E_L is the total energy of the hemicalixarene conjugate, and E_{Ag} is that of the Ag^+) yielded −142.7 kcal/mol.9

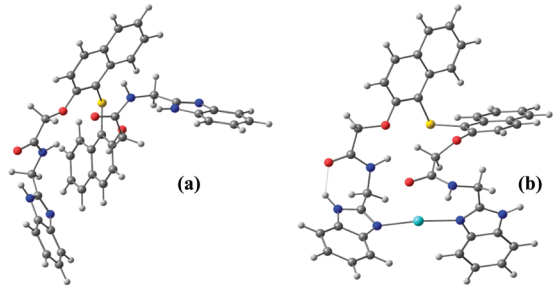

Figure 8. DFT-optimized structures of (a) **L** and (b) $[Ag^+-L]$. Bond distances (Å): N1−Ag = 2.17, N2−Ag = 2.20. Bond angle (deg): N1−Ag−N2 was found to be 169.

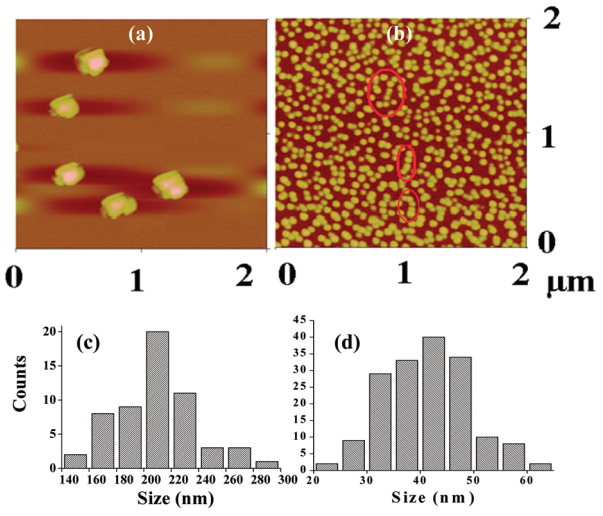

Figure 9. AFM micrographs of (a) **L** and (b) $[Ag^+-L]$. Few representative chain-like structures are encircled on (b). Distribution of the particle sizes observed in AFM for **L** in the absence (c) and in the presence (d) of Ag^+ ion.

Microstructural Features of L and Its Silver Complex by AFM and TEM. AFM images of **L** and its complex show that the particles were well spread over the mica sheet. The morphological features of **L** alone and in the presence of Ag^+ are quite distinct in both shape and size. While **L** alone forms large lumps, like aggregates of size 160−230 nm, such aggregation is inhibited and uniform spherical particles with

dx.doi.org/10.1021/jo201926q | J. Org. Chem. 2012, 77, 371−378

size of 30−60 nm are formed in the presence of Ag^+. Furthermore, the presence of Ag^+ induces the formation of chains of particles as shown in Figure 9. Thus, **L** has a tendency to form aggregates due to the presence of hydrophobic groups, and in presence of Ag^+, it forms linear chains as it could coordinate through benzimidazole nitrogens resulting in the breakage of the aggregations found in the simple **L**. In fact, similar chain formation of the particles has been observed in the AFM even when the control molecule possessing the benzimidazole moiety ($\mathbf{L}_4$) was treated with Ag^+ (SI 11). In effect, the structural features observed in AFM can indeed differentiate **L** from its complex of Ag^+.

Transmission electron micrographs of **L** show clusters of rod-like structures which were somewhat similar to the lumps observed in AFM. However, in the presence of Ag^+, multiple branched chain-like structures (Figure 10) were formed

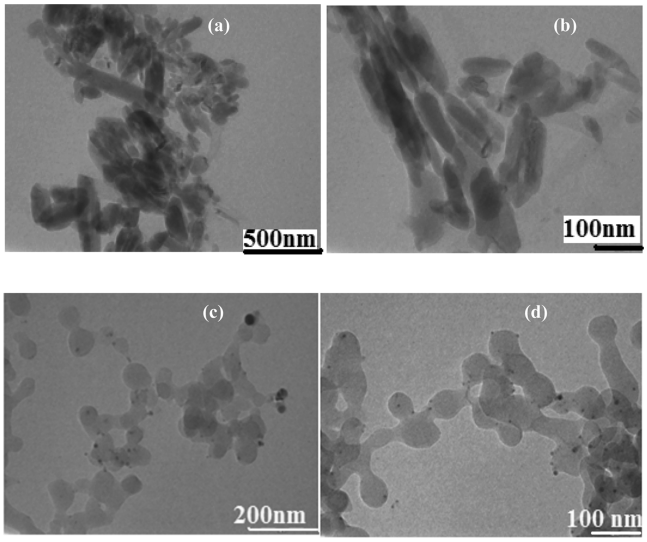

Figure 10. TEM micrographs shown in (a,b) are for **L** and shown in (c,d) are for [Ag^+−**L**].

through the aggregation of the spherical (40−60 nm) particles, which were analogues to those noticed in AFM. Thus, the structural alterations observed from nanoclusters to nanochains made up of nanospheres on going from the receptor to its Ag^+ complex are of importance in their applications,[9] while the mechanism of such transformation is still a matter of further research.

Secondary Sensor Behavior of [Ag^+−L] toward Amino Acids. Since **L** recognizes Ag^+ selectively, the utility of the [Ag^+−**L**] complex in the recognition of amino acids has been studied so that the complex can act as a secondary recognition entity.

Fluorescence and Absorption Titrations of [Ag^+−L] by Amino Acids. The chemosensing ensemble used in these titrations was prepared in situ by mixing **L** and Ag^+ in 1:2 ratio. The fluorescence intensity of [Ag^+−**L**] was quenched in the presence of Cys, Asp, and Glu and not with the other amino acids (SI 12). During the titration of [Ag^+−**L**] with Cys, the emission band observed at 390 nm is quenched (Figure 11). This is exactly reverse to what happens when **L** is titrated with Ag^+, indicating the removal of Ag^+ by Cys and thereby releasing the free **L**. This is true even with Asp and Glu, which possess carboxylate moieties (SI 13). Out of the 20 amino acids studied, Trp and Tyr did not yield interpretable results due to their strong emission that overlaps with the emission of **L** upon excitation at 280 nm. Thus the [Ag^+−**L**] complex acts as a secondary recognition ensemble toward Cys, Asp, and Glu.

Interaction of Ag^+ with Cys and the consequent release of **L** were further supported by UV−visible absorption spectroscopy carried out with [**L** + 2 equiv of Ag^+]. Absorption spectrum obtained after addition of Cys, Asp, and Glu to [Ag^+−**L**] is similar to the free **L** showing bands at 274, 280, and 343 nm, suggesting the release of **L** from the complex by Cys, Asp, and Glu (Figure 12) (SI 14).

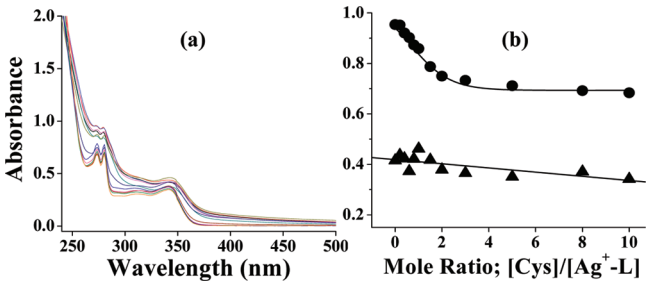

Figure 12. Absorption spectral titration of [Ag^+−**L**] with cysteine: (a) spectral traces; (b) absorbance vs mole ratio at 274 nm (circles) and 340 nm (triangles).

ESI-MS Titration of [Ag^+−L] with Cys, Asp, and Glu. In order to confirm the release of **L** and the recomplexation of Ag^+ by the amino acid, ESI-MS titrations were carried out between [Ag^+−**L**] complex and Cys, Asp, and Glu (SI 15). The mass spectra exhibited major peaks supporting Ag^+ complex of Cys (m/z = 348.1), Asp (m/z = 372.9), and Glu (m/z = 401.1) and further supporting the release of **L** (m/z = 693.2) in the titrations in the case of these amino acids. All of these clearly support the release of **L** and also the formation of the complex between Ag^+ and Cys, Asp, or Glu.1314

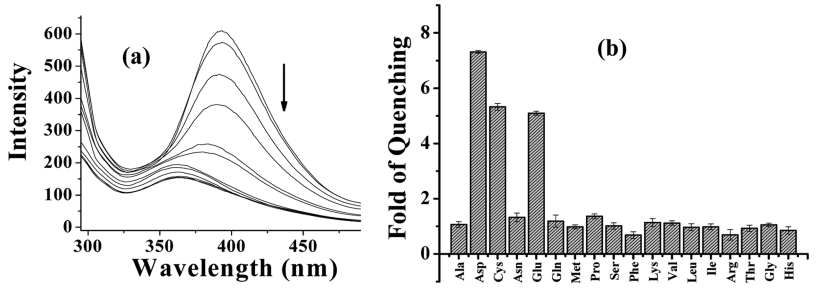

Figure 11. (a) Fluorescence spectral traces obtained during the titration of [Ag^+−**L**] with cysteine. Downward arrow shows the addition of 0 → 20 equiv of cysteine to [Ag^+−**L**]. (b) Histogram showing the fold of quenching of fluorescence of [Ag^+−**L**] in the presence of different amino acids.

dx.doi.org/10.1021/jo201926q | J. Org. Chem. 2012, 77, 371−378

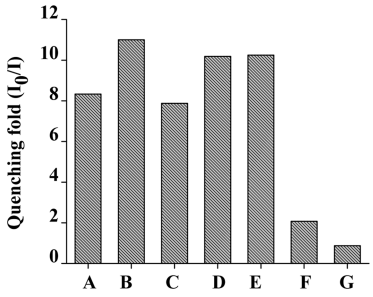

Figure 13. Histogram showing the fold of fluorescence quenching of the [Ag^+−**L**] complex by −SH as well −COOH containing molecules, where A = cysteine, B = ethyl ester of cysteine, C = cysteamine, D = glutathionine reduced (GSH), E = glutathionine reduced (GSSH), F = dimethyl glutamic acid ester, and G = dibenzyl ester of aspartic acid.

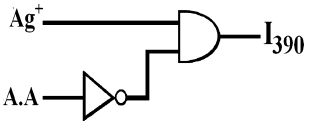

Ag^+	A.A	I_{390}
0	0	0
0	1	0
1	0	1
1	1	0

Figure 14. (a) Representation of INH logic gate using conventional gate notation; an active output signal is obtained when Ag^+ = 1 and amino acids (A.A), viz., Cys, Asp, or Glu = 0. (b) Truth table for INH logic gate, Ag^+ and A.A (Cys, Asp, or Glu) are input to the system; I_{390} is the output signal of **L** at 390 nm.

Role of Side Chains of Cys, Asp, and Glu in the Removal of Ag^+ from the Complex. Since the fluorescence and absorption changes occur only in the presence of Cys, Asp, and Glu and not with any other amino acid, the role of −SH and −COOH functional groups in the binding followed by the removal of Ag^+ was further confirmed by measuring the fluorescence and absorption response of the [Ag^+−**L**] complex with other −SH and −COOH blocked molecules, viz., cysteine ethyl ester, cysteamine, glutathionine reduced (GSH), glutathionine oxidized (GSSH), dimethyl glutamic acid ester, and dibenzyl aspartic acid ester (Figure 13). The results suggest that Ag^+ mainly interacts through −SH or −COOH functional groups. The [Ag^+−**L**] chemo ensemble acts a recognition medium for thiol and carboxylic acid functionality.

INH Logic Gate Properties of L with Ag^+ and Cys, Asp, and Glu. The logic gate properties of **L** have been studied using two sets of input signals, while one is Ag^+ and the other is an amino acid (Cys, Asp, and Glu), by monitoring the fluorescence emission at 390 nm. From the logic gate functions, the emission of **L** is observed only in the presence of single input, viz., Ag^+ and not with Cys, Asp, and Glu as these amino acids are insensitive to **L**. This indicates that **L** is ***switched on*** only in the presence of Ag^+ (7-fold enhancement at 390 nm). Similarly, in the presence of 2 equiv of Cys, Asp, or Glu, fluorescence emission of [Ag^+−L] was quenched and no significant output signal was observed. From these studies, it has been found that **L** can be used as INHIBIT (INH) logic gate toward Ag^+ in the absence of Cys, Asp, and Glu by observing emission at 390 nm. The truth table and the pictorial representation for the corresponding INH logic gate are given in Figure 14.

CONCLUSIONS

A thio-bridged hemicalixarene receptor system based on the benzimidazole arm (**L**) has been synthesized, characterized, and explored for its metal ion recognition property extensively using spectroscopic techniques. The derivative **L** showed selective *turn-on* fluorescence response toward Ag^+ in aqueous methanol [(7.5 ± 0.5)-fold] among the 14 different metal ions studied. The novelty of **L** in Ag^+ sensing has been confirmed by carrying out similar fluorescence titration with three control molecules, viz., L_1, L_2, and L_4. The complex formation, stoichiometry, and binding mode have been established by UV−vis, ESI-MS, and ^{1}H NMR studies and found to be 1:1. Moreover, the species of formation have been modeled using DFT computational calculations. The morphology changes observed on going from the simple receptor **L** to its Ag^+ complex by AFM and TEM were dramatic enough to differentiate the receptor from its Ag^+ complex. Thus, the morphological features of **L** alone and **L** in the presence of Ag^+ are distinctly different both in shape and size, forming aggregates of 160−230 nm size in the case of **L**, while such aggregation is inhibited by forming uniform spherical particles with a size of 30−60 nm in the presence of Ag^+. Further, these spherical particles merge together to form chains.

The in situ [Ag^+−**L**] complex was further explored for its secondary detection of amino acids resulting in selective *turn-off* response toward Cys, Asp, and Glu among the 20 naturally occurring ones, by interacting through −SH and −COOH side chain functionality, and thereby making the **L** and its silver complex systems interesting. The displacement of Ag^+ from the binding core of the complex of **L** upon addition of these amino acids has been confirmed by the ESI-MS titration. The results obtained in the present studies help to construct an INHIBIT logic gate.

EXPERIMENTAL SECTION

Synthesis and Characterization Data for the Compounds, L_1, L_2, L_3, L, and L_4. The derivatives have been prepared by following the procedures given below and were characterized.

Thiobis(2,2′-naphthol) (L_1). This was synthesized as per the reported procedure[10] with some modifications. To a solution of 2-naphthol (27.4 g, 190 mmol) in diethyl ether (400 mL) at 0 °C was added dropwise a solution of sulfur dichloride (6.00 mL, 94.6 mmol) in diethylether (100 mL). The resulting suspension was allowed to cool to room temperature and stirred for 24 h. The precipitate that formed was filtered, washed twice with 40 mL portions of diethyl ether, and dried: yield (16.23 g, 57%); mp 209−210 °C dec; FTIR (KBr, cm^{-1}) 3356, 3345, 1619, 1595, 1570. ^{1}H NMR (400 MHz, $CDCl_3$, δ ppm) 6.87 (s, 2 H, Ar−OH), 7.19 (d, 2 H, Ar−H, J = 8.92 Hz), 7.33 (t, 2 H, Ar−H, J = 8.12 Hz), 7.51 (t, 2 H, Ar−H, J = 8.28 Hz), 7.76 (d, 4 H, Ar−H, J = 8.48 Hz), 8.45 (d, 2 H, Ar−H, J = 7.88 Hz); ^{13}C NMR ($CDCl_3$, δ ppm) 156.8, 135.4, 130.5, 128.5, 127.1, 124.7, 123.8, 118.2, 112.5 (Nap-C); ESI-MS m/z (%), 318.15 (100, $[M]^+$); 175 (95). Anal. (%) Calcd for $C_{20}H_{14}O_2S$: C, 75.45; H, 4.43; S, 10.07. Found: C, 75.51; H, 4.41; S, 9.84.

1,1′-Thiobis(2-naphthoxy acetic ester) (L_2). In a 250 mL flask equipped with a magnetic stirrer and reflux condenser, a mixture of L_1 (20 g, 62.90 mmol), ethylbromoacetate (14.60 mL, 132.09 mmol), and potassium carbonate (9.95 g, 72.10 mmol) was added in 100 mL of dry acetone. Then the reaction mixture was heated at reflux temperature for 12 h under nitrogen atmosphere. After cooling, the mixture was filtered through a bed of Celite and the organic phase was evaporated to yield a white solid product. The solid product was dissolved in dichloromethane, washed with 10% sodium hydroxide, and the organic phase was evaporated. Recrystallization from methanol afforded pure L_2: yield (26.19 g, 85%); FTIR (KBr, cm^{-1}) 3040, 2970, 1750, 1595; ^{1}H NMR (400 MHz, $CDCl_3$, δ ppm) 1.15 (t, −COO−CH_2−, 4H, J = 7.20 Hz), 4.18 (q, 6H, $-CH_3$, J = 7.16 Hz), 4.37 (s, 4H, OCH_2), 7.02 (d, 2H, Ar−H, J = 8.92 Hz), 7.35 (t, 2H, Ar−H, J = 8.02 Hz), 7.47 (t, 2H, Ar−H, J = 8.32 Hz), 7.68 (d, 2H, Ar−H, J = 8.96 Hz), 7.72 (d, 2H, Ar−H, J = 8.08 Hz), 8.70 (d, 2H, Ar−H, J =

dx.doi.org/10.1021/jo201926q | J. Org. Chem. 2012, 77, 371−378

7.68 Hz); ^{13}C NMR ($CDCl_3$, δ ppm) 168.8, 156.4, 135.5, 128.5, 127.1, 124.7, 123.8, 119.2, 115.5 (Nap-C); 66.9, 61.1 ($-CH_2-CH_3$); 14.1 ($-CH_3$); ESI-MS m/z (%), 491 (80, $[M + H]^+$); 261 (100). Anal. (%) Calcd for $C_{28}H_{26}O_6S$: C, 68.55; H, 5.34; S, 6.54. Found: C, 68.42; H, 5.34; S, 6.21.

1,1′-Thiobis(2-naphthoxy acetic acid) (L_3). Into a 250 mL single-neck flask containing ethanol (100 mL) and L_2 (19 g, 38.76 mmol) was added 15% aqueous sodium hydroxide (42 mL, 158 mmol), and the mixture was heated to reflux for 24 h. After the reaction, the mixture was evaporated under reduced pressure to yield a white solid. The residue was diluted (suspension) with cold water, and hydrochloric acid (3 N) was added with vigorous mixing until pH 1 was reached. A white precipitate obtained was collected, washed with water, and dried. Pure L_3 was obtained after recrystallization from ethanol: yield (15.98 g, 95%); FTIR (KBr, cm^{-1}) 3210–2420 (br), 1720, 1710, 1620, 1430, 1275; ^{1}H NMR (400 MHz, DMSO-d_6, δ ppm) 4.83 (s, 4H, O–CH_2), 7.23 (t, 4H, Ar–H, J = 7.75 Hz), 7.37 (t, 2H, Ar–H, J = 8.20 Hz), 7.75 (d, 2H, Ar–H, J = 9.1 Hz), 7.85 (d, Ar–H, 2H, J = 7.76 Hz), 8.50 (d, 2H, J = 8.52 Hz), 13.15 (br, 2H, –COOH); ^{13}C NMR (DMSO-d_6, δ ppm) 170.8, 156.6, 135.3, 130.1, 129.6, 128.3, 127.1, 125.9, 124.3, 119.1, 115.1, 66.6; ESI-MS m/z (%), 457 (67, $[M + Na]^+$); 435 (46, $[M + H]^+$); 232 (100). Anal. (%) Calcd for $C_{24}H_{18}O_6S$: C, 66.35; H, 4.18; S, 7.38. Found: C, 66.28; H, 4.08; S, 7.14.

Synthesis of L. To a solution of L_3 (0.3 g, 0.690 mmol) in DMF (50 mL) were added Et_3N (0.5 mL, 3.46 mmol), 1-ethyl-(3-dimethylaminopropyl)-3-carbodiimide hydrochloride (0.40 g, 2.07 mmol), and catalytic amount of 1-hydroxybenzotriazole (HOBT), and the solution was stirred at 0 °C for 30 min under N_2 atmosphere. A hydrochloride salt of 2-aminomethyl benzimidazole (0.32 g, 1.4 mmol) was added to this reaction mixture and stirred at room temperature overnight. The resulting mixture was added with water (50 mL) and extracted in dichloromethane (100 mL × 2). The dichloromethane extract was washed with water followed by saturated $NaHCO_3$ and brine. The organic phase was evaporated to give white solid, **L**. The product was recrystallized from dichloromethane/methanol: yield (0.35 g, 73%); FTIR (KBr, cm^{-1}) 1686 ($\nu_{C=O}$); ^{1}H NMR (400 MHz, DMSO-d_6, δ ppm) 4.51 (s, 4H, NCH_2), 4.67 (s, 4H, OCH_2), 7.12 (br, 4H, Benz-H), 7.4 (m, 12H, Ar–H), 7.82 (t, 2H, CONH, J = 8.2 Hz), 8.44 (br, 4H, Ar–H), 12.71 (s, 2H, Benz-NH); ^{13}C NMR: (DMSO-d_6, δ ppm) 36.1, 68.6, 115.7, 117.5, 121.4, 124.2, 124.8, 127.3, 129.6, 130.1, 134.2, 151.8, 156.2, 168.1; ESI-MS m/z (%), 692 (100, $[M]^+$); HRMS (EI) calcd for $C_{40}H_{33}N_6O_4S$ m/z 693.2284, found m/z 693.2311.

Synthesis of Control Molecule L_4. To a solution of phenoxy-acetic acid (1 g, 6.5 mmol) in dry CH_2Cl_2 (60 mL) were added Et_3N (2.28 mL, 16.45 mmol), 1-ethyl-(3-dimethylaminopropyl)-3-carbodiimide hydrochloride (2.50 g, 13 mmol), and a catalytic amount of 1-hydroxybenzotriazole (HOBT), and then the solution was stirred at 0 °C for 30 min under N_2 atmosphere. A hydrochloride salt of 2-aminomethyl benzimidazole (1.5 g, 6.8 mmol) was added to this reaction mixture and stirred at room temperature overnight. The reaction mixture was concentrated by rotary evaporation, and solid crude product obtained was redissolved in CH_2Cl_2. The dichloromethane portion was washed with water (50 mL × 3) followed by brine and dried over anhydrous sodium sulfate, filtered, and solvent was removed by rotary evaporation. The solid crude product, L_4, was purified by silica gel column chromatography using ethyl acetate/petroleum ether (4:6 v/v) as eluent: yield (1.29 g, 71%); FTIR (KBr, cm^{-1}) 1667 ($\nu_{C=O}$), 1068; ^{1}H NMR (400 MHz, DMSO-d_6, δ ppm) 4.57–4.59 (2s, 4H, NCH_2 and OCH_2), 6.97 (t, 1H, Ar–H J = 7.36 Hz,), 7.02 (d, 2H, Ar–H, J = 7.84 Hz), 7.15 (m, 2H, Ar–H), 7.32 (t, 2H, Ar–H, J = 8.03 Hz,), 7.50 (br, 2H, Benz-H), 8.79 (t, 1H, CONH, J = 5.86 Hz), 12.25 (s, 1H, Benz-NH); ^{13}C NMR (DMSO-d_6, δ ppm) 37.6, 67.5, 115.4, 115.4, 121.9, 122.1, 130.2, 152.7, 158.3, 168.9; HRMS (EI) calcd for $C_{16}H_{16}N_3O_2$ m/z 281.1252, found m/z 281.1243.

Computational Studies. Computational studies were carried out using Gaussian 03 package.[11] Prior to assuming the initial guess model for computational calculations, structure of **L** was generated using gaussview from the single-crystal XRD structure of a similar methylene-bisnaphthalene-amidomethyl benzimidazole di-derivative.[12] The structure was then optimized by semiemprical methods followed by HF and then by DFT in a cascade fashion. In order to generate the metal complex, silver ion has been placed randomly at a distance that is far away from the benzimidazole region. The corresponding complex of **L** with Ag^+ was then optimized in a cascade fashion by going through AM1 → HF/3-21G → B3LYP/3-21G level of computation.

Fluorescence Titrations. All of the fluorescence titrations were carried out on a Perkin-Elmer LS55 at 280 nm excitation wavelength in 1 cm quartz cell. Bulk solutions (6×10^{-4} M) of **L** were freshly made before each set of experiments by dissolving the ligand in DMSO (50 μL) and then making up with the 2:3 methanol–water mixture. The metal perchlorate salts were made at 6×10^{-4} M concentration in 2:3 methanol–water mixture. The fluorescence titrations were carried by exciting the solution at 280 nm wavelength after adding an appropriate volume of metal salt solution to result in requisite mole ratios of $[M^{n+}]/[L]$, yet maintaining the final [**L**] as 10 μM in a total solution volume of 3 mL achieved by diluting with solvent.

Absorption Titrations. Bulk solutions were made by similar procedure as in fluorescence studies. Titrations were performed by varying equivalents of $[M^{n+}]$ from 0.2 to 10 and fixing the concentration of **L** at 35 μM.

^{1}H NMR Titration. **L** (0.01 M) was taken in NMR tube in DMSO-d_6 (400 μL) followed by addition of a varying quantity of Ag^+ (dissolved in DMSO-d_6).

Sample Preparations for AFM and TEM. For AFM studies, the stock solution of (**L**) and Ag^+ were taken as 6×10^{-5} M. The **L** was dissolved in methanol/water (2:3) system. The ligand to Ag^+ ratio was 1:2, and the system was sonicated for 10 min, after which 50–70 μL of aliquot was taken and spread over a mica sheet using the drop-cast method. The sample was then dried and subjected to AFM studies. For TEM studies, the sample preparation procedure followed for AFM was adopted except that the stock solution of **L** and Ag^+ used was 6×10^{-3} M. The samples were dispersed on a carbon-coated grid by drop-cast method.

■ ASSOCIATED CONTENT

Ⓢ Supporting Information

Synthesis and characterization including spectral data of **L** and its precursors, fluorescence and absorption data, minimum detection limit, and computational data. This material is available free of charge via the Internet at http://pubs.acs.org.

■ AUTHOR INFORMATION

Corresponding Author

*Phone: +91-22-2576-7162. Fax: +91-22-2572-3480. E-mail: cprao@iitb.ac.in.

■ ACKNOWLEDGMENTS

C.P.R. acknowledges the financial support from DST, CSIR, and DAE BRNS. Both A.M. and G.S.B. acknowledge CSIR, and K.T. acknowledges UGC for their fellowships. J.D. acknowledges DRDL for allowing to register for the Ph.D. program at IIT Bombay. We also acknowledge FIST (Physics)-IRCC central SPM facility of IIT Bombay for AFM studies.

■ REFERENCES

(1) (a) Ratte, H. T. *Environ. Toxicol. Chem.* **1999**, *18*, 89. (b) Butkus, M. A.; Labare, M. P.; Starke, J. A.; Moon, K.; Talbot, M. *Appl. Environ. Microbiol.* **2004**, *70*, 2848. (c) Petering, H. G. *Pharmacol. Ther. A* **1976**, *1*, 127. (d) Russell, A. D.; Hugo, W. B. *Prog. Med. Chem.* **1994**, *31*, 351. (e) Yakabe, Y.; Sano, T.; Ushio, H.; Yasunaga, T. *Chem. Lett.* **1980**, *4*, 373.

(2) Mcdonnell, G.; Russell, D. A. *Clin. Microbiol. Rev.* **1999**, *12*, 147.

(3) (a) Kang, J.; Choi, M.; Lee, E. Y.; Yoon, J. *J. Org. Chem.* **2002**, *67*, 4384. (b) Coskun, A.; Akkaya, E. U. *J. Am. Chem. Soc.* **2005**, *127*, 10464. (c) Shamsipur, M.; Alizadeh, K.; Hosseini, M.; Caltagirone, C.; Lippolis, V. *Sens. Actuators, B* **2006**, *113*, 892. (d) Tong, H.; Wang, L. X.; Ting, X. B.; Wang, F. *Macromolecules* **2002**, *35*, 7169. (e) Parker, J.; Glass, T. E. *J. Org. Chem.* **2001**, *66*, 6505. (f) Ishikawa, J.; Sakamoto, H.; Nakao, S.; Wada, H. *J. Org. Chem.* **1999**, *64*, 1913. (g) Huang, C.; Peng, X.; Lin, Z.; Fan, J.; Ren, A.; Sun, D. *Sens. Actuators, B* **2008**, *133*, 113. (h) Kim, S. K.; Lee, J. K.; Lee, S. H.; Lim, M. S.; Lee, S. W.; Sim, W.; Kim, J. S. *J. Org. Chem.* **2004**, *69*, 2877. (i) Lin, H.; Cinar, M. E.; Schmittel, M. *Dalton Trans.* **2010**, *39*, 5130. (j) Ray, D.; Iyer, E.; Siva, S.; Sadhu, K. K.; Bharadwaj, P. K. *Dalton Trans.* **2009**, 5683. (k) Hung, H. C.; Cheng, C. W.; Wang, Y. Y.; Chen, Y. J.; Chung, W. S. *Eur. J. Org. Chem.* **2009**, 6360. (l) Liu, L.; Zhang, D.; Zhang, G.; Xiang, J.; Zhu, D. *Org. Lett.* **2008**, *10*, 2271. (m) Kandaz, M.; Guney, O.; Senkal, F. B. *Polyhedron* **2009**, *28*, 3110. (n) Wang, H. H.; Xue, L.; Qian, Y. Y.; Jiang, H. *Org. Lett.* **2010**, *12*, 292.

(4) (a) Wang, F.; Nandhakumar, R.; Moon, J. H.; Kim, K. M.; Lee, J. Y.; Yoon, J. *Inorg. Chem.* **2011**, *50*, 2240. (b) Swamy, K.M. K.; Kim, H. N.; Soh, J. H.; Kim, Y.; Kim, S. J.; Yoon, J. *Chem. Commun.* **2009**, 1234. (c) Chatterjee, A.; Santra, M.; Won, N.; Kim, S.; Kim, J. K.; Kim, S. B.; Ahn, K. H. *J. Am. Chem. Soc.* **2009**, *131*, 2040. (d) Lin, C. Y.; Yu, C. J.; Lin, Y. H.; Tseng, W. L. *Anal. Chem.* **2010**, *82*, 6830. (e) Yang, R. H.; Chan, W. H.; Lee, A. W. M.; Xia, P.-F.; Zhang, H. K.; Li, K. A. *J. Am. Chem. Soc.* **2003**, *125*, 2884. (f) Lyoshi, S.; Taki, M.; Yamamoto, Y. *Inorg. Chem.* **2008**, *47*, 3946. (g) Park, C. S.; Lee, J. Y.; Kang, E. J.; Lee, J. E.; Lee, S. S. *Tetrahedron Lett.* **2009**, *50*, 671. (h) Schmittel, M.; Lin, H. *Inorg. Chem.* **2007**, *46*, 9139. (i) Xu, Z.; Zheng, S.; Yoon, J.; Spring, D. R. *Analyst* **2010**, *135*, 2554.

(5) Joseph, R.; Ramanujam, B.; Acharya, A.; Rao, C. P. *J. Org. Chem.* **2009**, *74*, 8181.

(6) Alvaro, M.; Garcia, H.; Palomares, E.; Achour, R.; Moussaif, A.; Zniber, R. *Chem. Phys. Lett.* **2001**, *350*, 240.

(7) Xia, C.-K.; Lu, C.-Z.; Zhang, Q.-Z.; He, X.; Zhang, J.-J.; Wu, D.-M.. *Cryst. Growth Des.* **2005**, *5*, 1569.

(8) Shockravi, A.; Chaloosi, M.; Rostami, E.; Heidaryan, D.; Shirzadmehr, A.; Fattahi, H.; Khoshsafar, H. *Phosphorus, Sulfur Silicon Relat. Elem* **2007**, *182*, 2115.

(9) Zhang, J.; Liu, J.; Peng, Q.; Wang, X.; Li, Y. *Chem. Mater.* **2006**, *18*, 867.

(10) (a) Gump, W. S.; Vitucci, J. C. *J. Am. Chem. Soc.* **1945**, *67*, 238. (b) Mercado, R. L.; Chandrasekaran, V.; Day, R. O.; Holmes, R. R. *Organometallics* **1999**, *18*, 906.

(11) Frisch, M. J.; et al. *Gaussian 03*, revision C.02; Gaussian Inc.: Wallingford, CT, 2004.

(12) Baghel, G. S.; Mobin, S. M.; Rao, C. P. *Inorg. Chim. Acta* **2009**, *362*, 2770.